Available online at www.sciencedirect.com
ScienceDirect
Ceramics International 35 (2009) 609–615
CERAMICS INTERNATIONAL
www.elsevier.com/locate/ceramint

Aqueous tape casting and crystallization kinetics of $Ce_{0.8}La_{0.2}O_{1.9}$ powder

Yen-Pei Fu [a,*], Sih-Hong Chen [a], Feng-Yi Tsai [a], Shao-Hua Hu [b]

[a] Department of Materials Science and Engineering, National Dong-Hwa University, Shou-Feng, Hualien 974, Taiwan
[b] Department of Environmental Resources Management, Dahan Institute of Technology, Sincheng, Hualien 971, Taiwan

Received 11 September 2007; received in revised form 15 December 2007; accepted 18 January 2008
Available online 24 April 2008

Abstract

An aqueous tape casting of $Ce_{0.8}La_{0.2}O_{1.9}$ (LDC) ceramics was developed using PAA as dispersant, PVA as binder, PEG as plasticizer, and deionized water as solvent. Surface properties of LDC powder with and without PAA dispersant were characterized by electrokinetic measurements. The rheology of the LDC slurries was evaluated with a rotary viscometer. The zeta potential measurement showed that the isoelectric point for LDC powders in the absence of dispersant corresponds to a pH value of 4.02. The experimental results showed the pH value greatly affects the rheology of the slurry. The optimum content to get a stable dispersed slurry is 1.5 wt% PAA at pH value of 9–10. In presence of 1.5 wt% PAA dispersant, 5 wt% PVA binder, 5 wt% PEG plasticizer, and 55 wt% LDC powders exhibited shear thinning behavior, indicating that LDC slurry was homogenous and well stabilized. With an appropriate formulation homogeneous, smooth, and defect-free green tapes were successfully obtained. Moreover, the crystallization kinetics of LDC powders prepared by coprecipitation process also has been investigated in this study. The activation energy of crystallization was calculated on the basis of differential scanning calorimetry (DSC) at different heating rates. From non-isothermal DSC data presented values in the range of 343.3–379.1 kJ/mol and 2.282–2.030 for the activation energy of crystallization and the Avrami exponent, respectively, at specific temperatures ranging from 280 to 285 °C.

Keywords: A. Powder: chemical properties; A. Tape casting; C. Thermal properties; D. CeO_2; E. Fuel cells

1. Introduction

Solid oxide fuel cells (SOFCs) are attracting widespread attention due to their high-energy conversion efficiency and low pollution. High oxide ionic conducting solid electrolytes based on zirconia have been intensively investigated [1]. In order to reduce the operation temperature from 1000 to 800 °C or even lower, doped ceria has been considered as the solid electrolyte for moderate temperature solid oxide fuel cells [2]. In contrast to pure zirconia, $CeO_{2-\delta}$ has the fluorite structure with oxygen vacancies ($V_O^{\bullet\bullet}$) as the predominant ionic defects. The oxygen vacancy concentration and concomitant oxide ion conductivity, in CeO_2 can be increased by the substitution of a lower valent metal such as Y [3], Sm [4,5], Gd [6,7], Y [8,9] and Ca [10]. Pure stoichiometric CeO_2 ceramics are poor oxide ion conductors. However, the ion conductivity can be significantly improved by increasing the oxygen vacancies by the substitution of lanthanum, which is lower than 4+ in valence and upon substituting for Ce^{4+} are charge compensated by oxygen vacancies, for example,

$$La_2O_3 \xrightarrow{CeO_2} 2La'_{Ce} + 3O_O^x + V_O^{\bullet\bullet}$$

In general, decreasing the thickness of the electrolyte can further reduce the resistance to ionic transport and allows lower operating temperature of SOFCs [11]. Tape casting is mainly used to manufacture thin flat ceramic sheets. The thickness of tape cast products is typically 20 μm to a few millimeters. Typical applications include transducers, capacitors, pyroelectric infrared detectors and SOFC [12]. Accordingly, we chose tape casting as a way to produce the electrolyte film of LDC for SOFC in this study.

Traditionally, tape casting was done using organic solvents. Because of environmental, health, safety, and economic reasons, aqueous media are substituting organic solvents [13]. Although, aqueous tape casting presented above-mentioned advantages, there are still several problems to overcome such as higher crack sensitivity, slow drying of the tape,

* Corresponding author. Tel.: +886 3 863 4209; fax: +886 3 863 4200.
E-mail address: d887503@alumni.nthu.edu.tw (Y.-P. Fu).

0272-8842/$34.00
doi:10.1016/j.ceramint.2008.01.018

flocculation and poor wetting of the slips [14,15]. The stability and rheological properties of ceramic suspension are influenced by many factors, such as pH, type and amount of dispersant and, the number of active groups on the powder surface. The stability and rheological properties of nanosized ceramics powders are more complex due to the particle interactions [16,17]. The rheological behavior of the slurries with addition of dispersant, binder, and plasticizer is studied. The stability of LDC suspension influenced by pH is also investigated in this study. Moreover, we also used coprecipitation process to produce GDC powder and studied its crystallization kinetics.

2. Experimental procedures

2.1. Starting materials

$Ce_{0.8}La_{0.2}O_{1.9}$ (LDC) was synthesized by a coprecipitation method. The detailed procedure is described as follows. Stoichiometric amounts of cerium nitrate hexahydrate ($Ce(NO_3)_3{\cdot}6H_2O$), and lanthanum nitrate hexahydrate ($La(NO_3)_3{\cdot}6H_2O$) were dissolved in distilled water. The final concentration of the stock solution was 0.2 M for Ce^{3+}. Then the ammonia (NH_4OH) solution was added to nitrates solution until pH 9.5, precipitates were formed. The resulting precipitate was vacuum-filtered, washed three times with water and ethanol, respectively. Then, the precipitate was dried at 80 °C in an oven. The coprecipitated hydrate powder decomposed to a polycrystalline oxide by heating to 600 °C for 2 h. The oxidation of Ce^{3+} to Ce^{4+} occurred during this stage. Deionized water was used as solvent. Poly(acrylic acid) (PAA) with molecular weight of (5000 g/mol) was used as an electrosteric dispersant. Poly(ethylene glycol) (PEG) with molecular weight of (400 g/mol) was used as plasticizer. Poly(vinyl alcohol) (PVA) with molecular weight of (13,000–18,000 g/mol) was used as binder. All organic additives are soluble in deionized water. The content of organic components in this study was expressed in weight percent with respect to the LDC powder.

2.2. Differential scanning calorimetry measurements

Differential scanning calorimetry (DSC; Model TG-DTA/DSC Setaram, Caluire, France) was used to study the crystallization characterization of coprecipitated LDC powder. A heating rate of 10–25 °C/min was used in DSC measurements up to 600 °C in air. Thermal analysis is done under flowing air at 100 ml/min. An initial sample weight of 12.0 ± 0.2 mg was used in all measurements. In this study, DSC instrument was calibrated using Sn. The melting temperature and latent heat of transformation for Sn are 231.8 °C and 60.46 J/g, respectively. The peak area values and onset temperatures were determined by a test run. These values were inputted and calculated by the software. It automatically revealed the correction data. We can use this correction data to correct our future data collected by the instrument.

2.3. Zeta potential measurements

In order to realize the relationship between dispersant amount of PAA with zeta potential, the zeta potential of suspension was measured using a Malvern Zetasizer nano-series. The suspensions were prepared by dispersing LDC powders (0.01 vol%) in deionized water. The pH value of suspension was adjusted by adding HNO_3 (0.1 M) or NH_4OH (1 M). The suspensions were mixed ultrasonically before the test to ensure that only the mobility of single particle was measured.

2.4. Rheological characteristic of slurry

Viscosity measurements were at room temperature performed using a rotary viscometer (BROOKFIELD DV-II$^+$ Pro viscometer). LDC suspensions were prepared at solid loadings in the range of 50–60 wt% containing the optimum amount of PAA.

2.5. Slurry preparation and tape casting

The tape cast slurries were prepared in two stages. First, LDC powder and deionized water with optimum content of dispersant were mixed in a polyethylene jar with ZrO_2 balls for 18 h. Next, the binder and plasticizer solution were milled for 18 h to obtain good homogeneity. Subsequently, the slurry was vacuumed to deair. Tape casting slurries were prepared by varying the weight of dispersant and ceramic powder. The slurries composition is given in Table 1. Tape casting was achieved using a laboratory-scale with a moving casting head on mylar substrate film. After tape casting, the tapes were left to dry at room temperature. The optimum composition of slurry is listed in Table 2.

2.6. Characterization techniques

A computer-interfaced X-ray powder diffractometer (XRD) with Cu Kα radiation (λ = 1.5418 Å) (Model Rigaku D/Max-II, Tokyo, Japan) was used to identify the crystalline phases. The

Table 1
Slurry composition at different weight of dispersant and ceramic powder

Component	Composition (wt%)		
	1	2	3
Ceramic powder	50	55	60
Dispersant	1.5	1.5	1.5
Binder	4.5	4.5	4.5
Plasticizer	4.5	4.5	4.5
Solvent	39.5	34.5	29.5

Table 2
Slurry formulation of aqueous tape casting LDC

Additive	Function	Content (wt%)
LDC	Ceramic powder	55.0
PAA	Dispersant	1.5
PVA	Binder	4.5
PEG	Plasticizer	4.5
Deionized water	Solvent	34.5

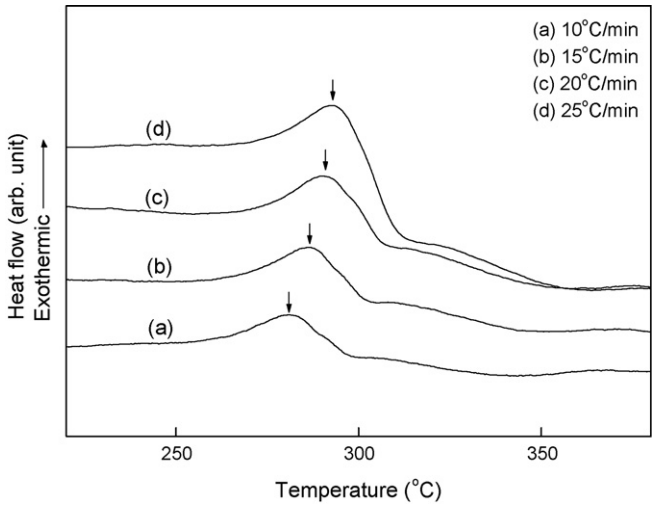

Fig. 1. Differential scanning calorimetry curves of coprecipitated $Ce_{0.8}La_{0.2}O_{1.9}$ powder at heating rates of 10, 15, 20, and 25 °C/min, respectively.

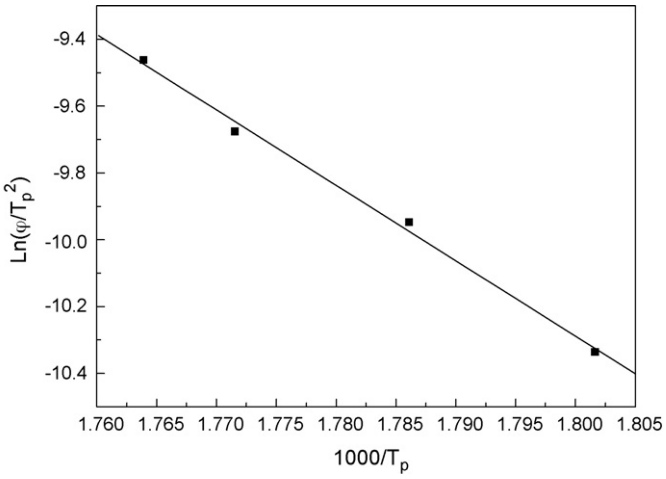

Fig. 2. Plot of $\ln(T_p^2/\Phi))$ against $1000/T_p$ for determining the value of crystallization activation energy for $Ce_{0.8}La_{0.2}O_{1.9}$.

morphological features of the green tape were observed using a scanning electron microscope (SEM; Model Hitachi S-3500H, Tokyo, Japan).

3. Results and discussion

3.1. Activation energy of crystallization

Fig. 1 shows the DSC curves of a sample for different heating rates ranging from 10 to 25 °C/min. With increasing heating rate, the exothermic peak shifts to a higher temperature. The crystallization peaks depending on different heating rates can be used to estimate the activation energy of crystallization. The activation energy of crystallization can be estimated by using the following Kissinger analysis [18]. Through the change in the peak crystallization temperature (T_p) with respect to heating rate, the activation energy of crystallization could be determined by using the Kissinger equation as follows:

$$\ln\left(\frac{T_p^2}{\Phi}\right) = \frac{E}{RT_p} + \text{constant} \quad (1)$$

where, E is the activation energy of crystallization. T_p is the temperature corresponding to the maximum of the DSC crystallization peak, R is the gas constant (8.314 J/mol), and Φ is the heating rate, which is 10, 15, 20, and 25 °C/min. The slope of the plot of $\ln(T_p^2/\Phi))$ versus $1/T_p$ should be a straight line, the slope should be E/R, and the activation energy of the crystallization process could be estimated. Fig. 2 shows the Kissinger plot of the coprecipitated LDC powder. The activation energy of crystallization is determined using the Kissinger from the slope and is equal to 187.6 kJ/mol.

Moreover, the Avarami exponent n can be determined from the DSC results. The value of the Avrami parameter n, which is a measure of the dimensionality of transformation, is determined using the Ozawa equation [19]:

$$\frac{d\{\ln[-\ln(1-X)]\}}{d\ln\Phi} = -n \quad (2)$$

In this equation, Φ denotes the heating rate, X is the volume fraction crystallized at a specified temperature T, X is the ratio of the partial area crystallized at a certain temperature to the total area of the crystallization exotherm. Here, the total area of the crystallization exotherm ranges between the temperature T_i at which crystallization just begins and the temperature T_f at which the crystallization is complete. The partial area crystallized at a certain temperature corresponds to the fraction located between T_i and T [20]. A plot of $\ln[-\ln(1-X)]$ versus $\ln\Phi$ should be a straight line. Then, n can be calculated from the slope of the plot. A value of n close to 3 indicates bulk or three-dimensional crystal growth and a value close to 1 indicates surface growth. Intermediate values of n between 1 and 3 indicate that surface and internal crystallizations occur simultaneously [21]. The Ozawa plot of $\ln[-\ln(1-X)]$ versus $\ln\Phi$ is shown in Fig. 3. Here, the volume fraction crystallized was calculated at a specific temperature in range of 280.0–285.0 °C. The value of n determined from the slope of the plot was 2.282, 2.078, and 2.030 for 280.0, 282.5, and 285.0 °C, respectively.

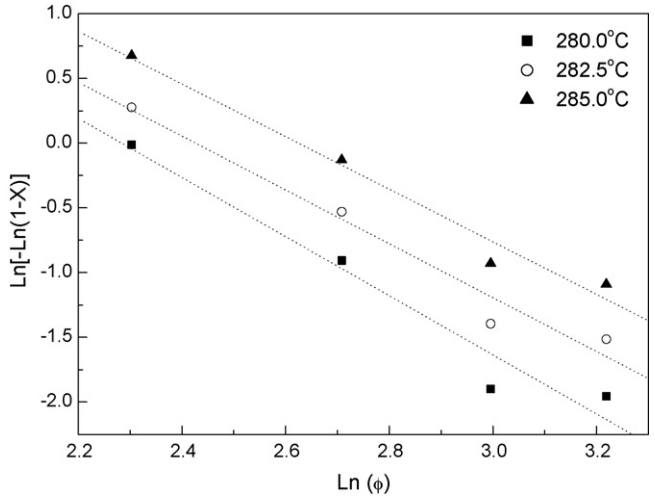

Fig. 3. Plot of $\ln[-\ln(1-X)]$ versus $\ln\Phi$ for the calculation of Avrami constant n values.

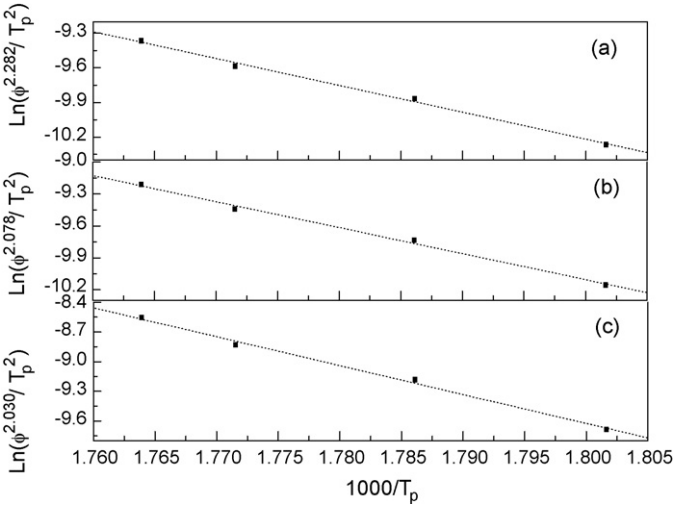

Fig. 4. Plot in accordance with the Matusita and Sakka equation for the determination of the activation energy for crystallization at specific temperature (a) 280.0 °C with $n = 2.282$, (b) 282.5 °C with $n = 2.078$, and (c) 285.0 °C with $n = 2.030$.

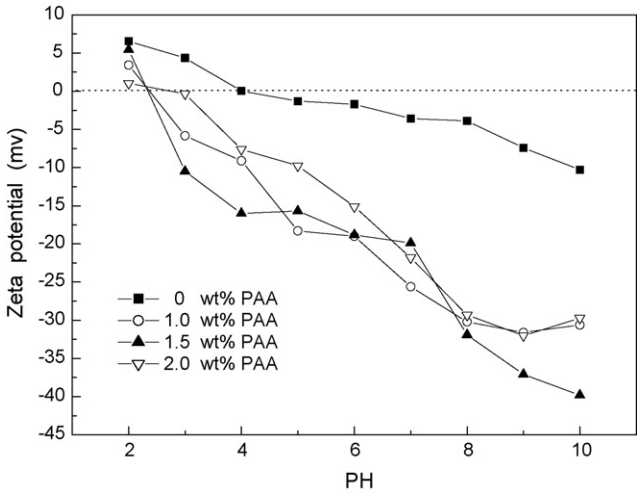

Fig. 5. Zeta potential of LDC powder as a function of pH after addition of various amounts of dispersant.

These results suggested that the crystallization is dominated by surface and internal simultaneously.

Matusita and Sakka proposed that the Kissinger model is valid only when crystal growth occurs on a specific number of nuclei [22,23]; otherwise, incorrect values for the activation energy are obtained. Therefore, they modified the Kissinger equation to account for nucleation and crystallization growth occurring simultaneously according to

$$\ln\left(\frac{\Phi^n}{T_p^2}\right) = -\frac{mE_c}{RT_p} + \text{constant} \quad (3)$$

where E_c is the activation energy of crystallization and m represents the dimensionality of the crystalline phase. n and m are related the relation $m = n - 1$. Fig. 4(a)–(c) shows the Matusita and Sakka plot for the determination of the activation energy of crystallization. Applying the modified Kissinger model, the activation energies of crystallization obtained lie in the range of 343.3–379.1 kJ/mol. The values of n and of the activation energy are given in Table 3.

3.2. Suspension stability

Zeta potential measurements were performed to identify the optimum pH value and dispersant content for LDC suspension as shown in Fig. 5. In the absence of dispersant the isoelectric point (IEP) was about 4.02. This value is very close to literature report. Luo et al. reported that 10 mol%-Gd_2O_3-doped CeO_2 nano-particles have an IEP at pH 4.4 [13]. The maximum zeta potential (absolute value) does not exceed 35 mV in the pH range of 3–8, indicating that the electrostatic repulsion between LDC particles is insufficient for stabilizing suspension in the absence of dispersant. For the suspension containing 1.5 wt% PAA dispersant, the maximum zeta potential (absolute value) was close to 40 mV in the pH range of 9–10. Therefore, we used a content of 1.5 wt% PAA for the tape casting slurry preparation. Noticeably, the dispersant amount greatly affects the interaction between LDC particles in aqueous suspensions. The function groups of PAA consist of carboxylic acid (COOH) groups, which can exist as COOH or dissociate to COO^-. The dissociation is written as follows,

$$\text{A-COOH} + H_2O \leftrightarrow \text{A-COO}^- + H_3O^+ \quad (4)$$

Depending on the pH and ionic strength of the solvent, the fraction of function of groups which are dissociated (COO^-) and those which are not dissociated (COOH) will alter. With increasing the fraction dissociated, the electrical charge on the polymer changes from neutral to highly negative. As the pH increases, the extent of dissociation and negative charge of the polymer increase for PAA. Then pH increases, a more negative charge adsorbs on the particles surface. It makes the zeta potential move negative. In this paper, an aqueous solution of PAA was used as an electrostatic dispersant. This PAA can aid ceramic dispersion because of the presence of non-adsorbed PAA species in solutions; the surface was measured to be 58 dyn/cm by the Wilhelmy method [24].

According to the literature, metal ions on the surface oxide layer behave as Lewis acids [25]. In presence of water, they may tend to coordinate H_2O molecules. Most oxide surfaces are hydrated and for a metal oxide, there will be MOH groups on the surface [26]. Fig. 6 illustrates the surface charge on CeO_2 particles below or beyond IEP. Below IEP, adsorption of H^+ ions leads a positively charged surface, whereas beyond IEP, adsorption of OH^- ions produces a negatively charged surface. Therefore, in this case, the dissociative chemisorption of water

Table 3
Crystallization parameters of LDC at various temperatures

Temperature (°C)	Avrami constant (n)	E_a (kJ/mol)
280.0	2.282	343.3
282.5	2.078	371.0
285.0	2.030	379.1

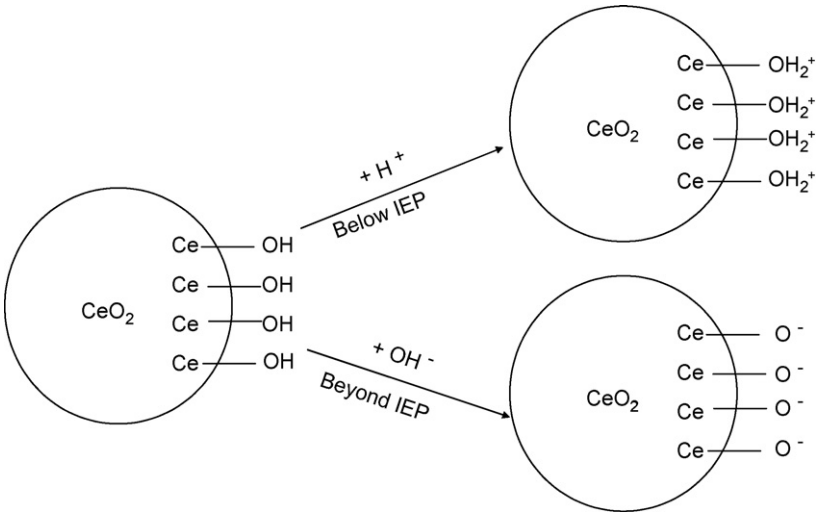

Fig. 6. The production of surface charges on CeO_2 particles by adsorption of ions from acidic or basic solutions.

molecules led to a hydroxyl group on surface, which is known to specifically adsorb H^+ and OH^- according to the following equation [25]:

$$\equiv Ce{-}OH + H^+ \leftrightarrow \equiv Ce{-}OH_2{}^+ \quad K_1 = \frac{[Ce{-}OH_2^+]}{[\equiv Ce{-}OH][H^+]} \tag{5}$$

$$\equiv Ce{-}OH + OH^- \leftrightarrow \equiv Ce{-}O^- + H_2O$$
$$K_2 = \frac{[Ce{-}O^-]}{[\equiv Ce{-}OH][OH^-]} \tag{6}$$

$$H_2O \leftrightarrow H^+ + OH^- \quad K_3 = [H^+][OH^-] \tag{7}$$

where K_3 is the equilibrium constant for the dissociation of H_2O, which is referred to as the ionic product of water. At the IEP $[Ce{-}OH_2^+]=[Ce{-}O^-]$ so that

$$[H^+]_{IEP} = \left(\frac{K_2K_3}{K_1}\right)^{1/2} \tag{8}$$

Since pH is defined as $pH=-\log[H^+]$, the IEP of LDC can be written as:

$$pH_{IEP} = \frac{14 + \log K_1 - \log K_2}{2} \tag{9}$$

It is obviously, that pH_{IEP} depends on the values of K_1, K_2 and K_3, which are related to the surface chemistry of the powder.

With $pH_{IEP} = 4.02$, are obtained form Eq. (9).

$$\frac{\log K_1 - \log K_2}{2} = -2.98$$

$$\frac{K_1}{K_2} = 10^{-5.96}$$

From above result, it indicates that K_2 great larger than K_1, implying that Eq. (6) dominates the reaction during the chemisorption process. This phenomena can be presumed that the surface $\equiv Ce{-}OH_2^+$ sites were withdrew and created $\equiv Ce{-}O^-$ site at equilibrium in water. According to the surface properties of CeO_2, polyelectrolyte PAA is selected as dispersant.

3.3. Properties of aqueous tape casting LDC slurries

According to Zeta potential measurements, a dispersant amount of 1.5 wt% PAA was used for stabilization of slurry containing 50, 55, 60 wt% LDC powder, with an adjusted pH of 9–10. Figs. 7 and 8 exhibit viscosity plots for LDC slurries at 50, 55, 60 wt% loading as a function of shear rate. The results reveal that the viscosity of slurries decrease versus increasing shear rate, typical of ''shear thinning'' behavior. This behavior is due to the attractive interaction of particles and the resultant formation of flocs in the slurry. Shear thinning fluid is favorable to arrange particles in slurry. Therefore, this fluid is preferred in tape casting because it reduces the mobility of constituents in the tape and preserves homogeneity of slurry [27]. All the slurries showed a shear thinning behavior with almost no time dependence effect. The maximum viscosity corresponds to 60 wt% solid loading, this formula being too viscous to be used

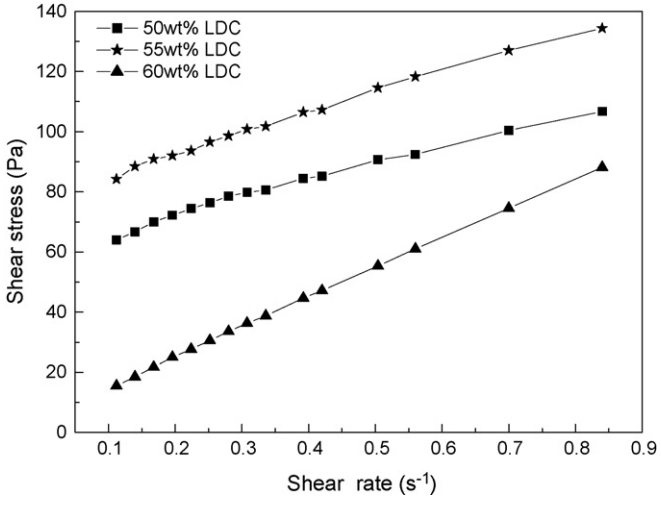

Fig. 7. Rheological curves of LDC slurries containing 1.5 wt% PAA.

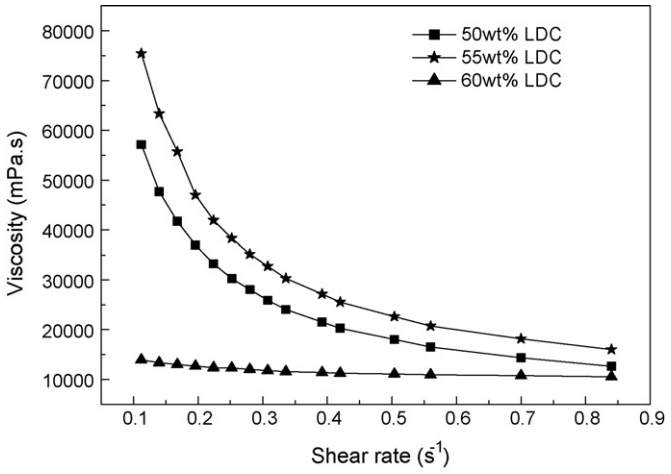

Fig. 8. Viscosity curves of suspensions containing different amounts of LDC powder loading with 1.5 wt% PAA as a function of shear rate.

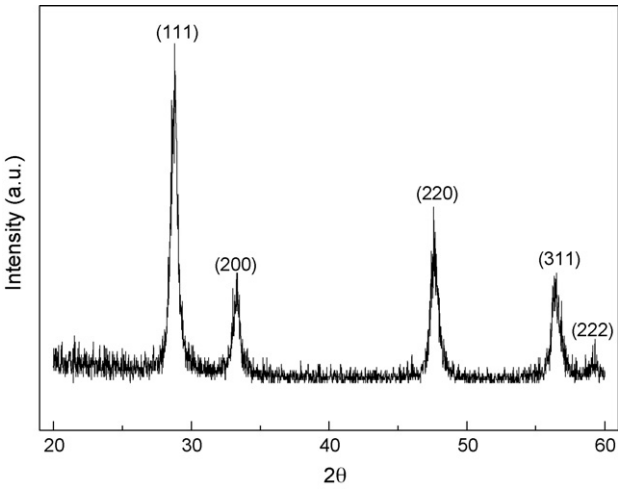

Fig. 9. XRD patterns for aqueous LDC green sheet.

for tape casting. Contrarily, the slurry with 50 wt% solid loading showed the lowest viscosity, but was unsuitable for tape casting. Accordingly, from experimental results, it was concluded that the optimum composition of slurry included, LDC powder 55 wt%, PAA 2 wt%, PVA 4.5 wt%, PEG 4.5 wt%, and deionized water 34 wt%. The relationship between the viscosity and shear rate can be expressed by the Herschel–Bulkley model [28]:

$$\eta = \frac{\tau_Y}{\dot{\gamma}} + K\dot{\gamma}^{n-1}$$

where τ_Y is the yield shear stress necessary to initiate flow, $\dot{\gamma}$ is shear rate, K is the consistency index and n is the shear thinning constant [29]. For a Newtonian behavior, $n = 1$, for a dilatant behavior, $n > 1$, and for a pseudoplastic behavior, $n < 1$. τ_Y, K, and n determined according to this equation, are listed in Table 4. Slurry with 55 wt% LDC revealed the lowest n value, the highest yield shear stress and k values among the three slurries formula. All LDC slurries exhibited pseudoplastic behaviors. From experimental results, it is concluded that the optimum composition of slurry was determined as, LDC powder 55 wt%, PAA 1.5 wt%, PVA 5 wt%, PEG 5 wt%, and deionized water 33.5 wt%.

3.4. Characteristics of green tapes

Fig. 9 reveals the X-ray diffraction patterns of aqueous $Ce_{0.8}La_{0.2}O_{1.90}$ green tape. The figure indicates that it contains only the cubic fluorite structure with space group *Fm*3*m*, no other crystalline phase is detected. All the peaks in the pattern match well with the Joint Committee of Powder Diffraction Standard (JCPDS) card file No. 34-0394. The microstructure of the green sheets of LDC is shown in Fig. 10. Both sides (top and bottom surface) of the tapes display very smooth surface. The

Table 4
Calculated τ_Y, K and n values of LDC slurries according to the Herschel–Bulkley equation

LDC content (wt%)	τ_Y (mPa)	K (mPa)	n
50	5.15	10523.2	0.230
55	106.19	12610.8	0.189
60	21.87	10003.3	0.859

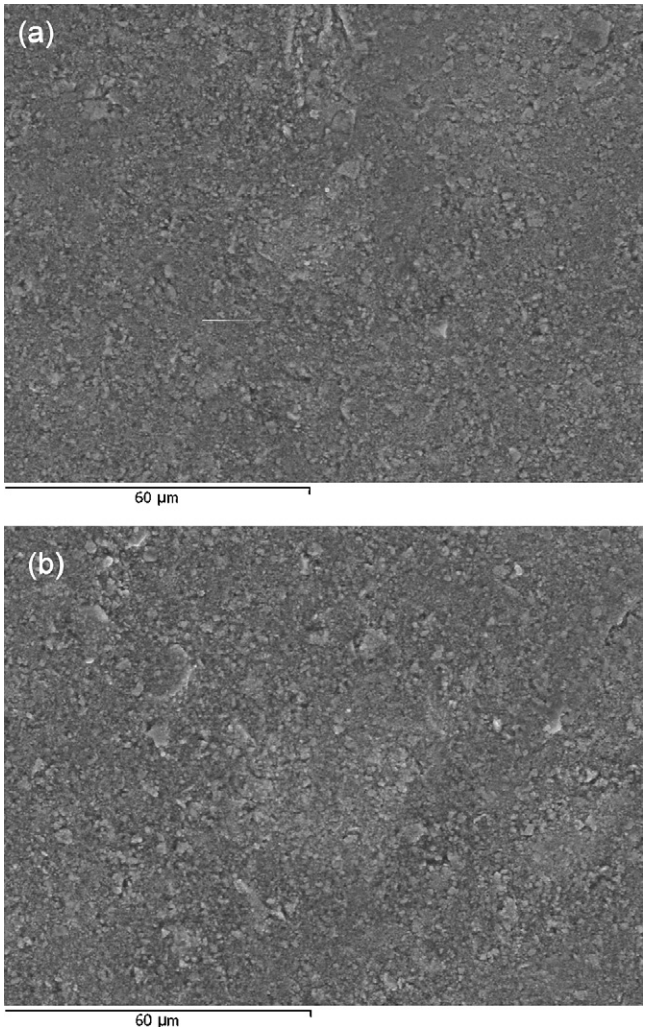

Fig. 10. SEM micrographs of LDC for dried tapes (a) top surface and (b) bottom surface.

homogeneity of the particle packing is ascribed to the fact that the LDC suspensions were well dispersed.

4. Conclusions

In this study, using PAA as dispersant, PVA as binder, PEG as plasticizer, and deionized water as solvent, flexible and smooth LDC tapes have been successfully prepared by tape casting process. The zeta potential measurement revealed that IEP for LDC powders in the absence of dispersant was 4.02. For aqueous LDC suspensions, the pH value greatly affects the rheology of the slurries. Optimum pH value of the slurry is in the range 9–10. Slurries containing 1.5 wt% PAA, 5 wt% PVA, 5 wt% PEG, and 55 wt% LDC powder exhibit shear thinning behavior, indicating that the slurry is homogenous and well stabilized. The homogeneous particle packing corresponds to the shear thinning behavior of the slurries. Both sides of the green tapes revealed smooth surfaces. No cracks were detected. Moreover, a non-isothermal study of crystallization kinetics of coprecipitated LDC was carried out by DSC measurements. The activation energy of crystallization is determined using the method proposed by Kissinger and is equal to 187.6 kJ/mol. The Avrami exponent n related to the dimensionality of crystal growth was determined using the Ozawa equation. The results reveal that the values of the n obtained experimentally are in the range of 2.282–2.030 for the specific temperature ranging from 280.0 to 285.0 °C. It is found that the controlling mechanism of crystallization is surface and internal growth simultaneously. By applying the modified Kissinger model, the activation energies of crystallization are obtained in the range of 343.3–379.1 kJ/mol.

Acknowledgement

The authors would like to thank the National Science Council of Taiwan for financial support (NSC 95-2221-E-259-023 and NSC 96-2221-E-122-001).

References

[1] B.C.H. Steele, Oxygen transport and exchange in oxide ceramics, J. Power Source 49 (1994) 1–3.
[2] N.Q. Minh, Ceramic fuel cells, J. Am. Ceram. Soc. 76 (1993) 563–588.
[3] H. Yahiro, Y. Baba, K. Eguchi, H. Arai, High-temperature fuel cell with ceria-yttria solid electrolyte, J. Electrochem. Soc. 135 (1988) 2077–2080.
[4] T. Inoue, T. Setoguchi, K. Eguchi, H. Aria, Study of a solid-oxide fuel cell with a ceria-based solid electrolyte, Solid State Ionics 35 (1989) 285–291.
[5] C.C. Chen, M.M. Nasrallah, H.U. Anderson, Synthesis and characterization of $(CeO_2)_{0.8}(SmO_{1.5})_{0.2}$ thin films for polymeric precursors, J. Electrochem. Soc. 140 (1993) 3555–3560.
[6] H. Yahiro, K. Eguchi, H. Aria, Electrical properties and reproducibilities of ceria-rare-earth oxide systems and their application to solid oxide fuel cell, Solid State Ionics 36 (1989) 71–75.
[7] D.L. Maricle, T.E. Swarr, S. Karavolis, Enhanced ceria-a low temperature SOFC electrolyte, Solid State Ionics 52 (1992) 173–182.
[8] E. Suda, B. Pacaud, M. Mori, Sintering characteristic, electrical conductivity and thermal properties of La-doped ceria powders, J. Alloys Compound 408–412 (2006) 1161–1164.
[9] Y.P. Fu, Microwave-induced combustion synthesis and ion conductivity of $Ce_{1-x}La_xO_{2-1/2x}$ ceramics, Jpn. J. Appl. Phys. 45 (2006) 5996–5999.
[10] R.N. Blumenthal, F.S. Brugner, J.E. Garnier, The electrical conductivity of CaO-doped nonstoichiometric cerium dioxide from 700 to 1500 °C, J. Electrochem. Soc. 120 (1973) 1230–1237.
[11] J. Cheng, S. Zha, X. Fang, X. Liu, G. Meng, On the green density, sintering behavior and electrical property of tape cast $Ce_{0.9}Gd_{0.1}O_{1.95}$ electrolyte film, Mater. Res. Bull. 37 (2002) 2437–2446.
[12] A. Navarro, J.R. Alcock, R.W. Whatmore, Aqueous colloidal processing and green sheet properties of lead zirconate titanate (PZT) ceramics made by tape casting, J. Eur. Ceram. Soc. 24 (2004) 1073–1076.
[13] L.H. Luo, A.I.Y. Tok, F.Y.C. Boey, Aqueous tape casting of 10 mol%-Gd_2O_3-doped CeO_2 nano-particles, Mater. Sci. Eng. A 429 (2006) 266–271.
[14] T. Chartier, A. Bruneau, Aqueous tape casting of alumina substrates, J. Eur. Ceram. Soc. 12 (1993) 243–247.
[15] J.X. Zhang, D.L. Jiang, S.H. Tan, L.H. Gui, M.L. Ruan, Aqueous processing of titanium carbide green sheets, J. Am. Ceram. Soc. 84 (2001) 2537–2541.
[16] Y. Liu, L. Gao, Effect of 2-phosphonobutane-1,2,4-tricarboxylic acid adsorption on the stability and rheological properties of aqueous nano-sized 3-mol%-yttria-stabilized tetragonal-zirconia polycrystal suspensions, J. Am. Ceram. Soc. 87 (2003) 1106–1113.
[17] J.A. Lewis, Colloidal processing of ceramics, J. Am. Ceram. Soc. 83 (2000) 2341–2359.
[18] H.E. Kissinger, Variation of peak temperature with heating rate in different thermal analysis, J. Res. Natl. Bur. Stand. (U.S.) 57 (1956) 217–221.
[19] T. Ozawa, Kinetic of non-isothermal crystallization, Polymer 12 (1971) 150–158.
[20] C.T. Cheng, M. Lanagan, B. Jones, J.T. Lin, M.J. Pan, Crystallization kinetic and phase development of PbO-BaO-SrO-Nb_2O_5-B_2O_3-SiO_2-based glass-ceramics, J. Am. Ceram. Soc. 88 (2005) 3037–3042.
[21] A.A. Francis, Non-isothermal crystallization kinetics of a blast furnace slag glass, J. Am. Ceram. Soc. 88 (2005) 1859–1863.
[22] K. Matusita, S. Sakka, Kinetics study of crystallization of glasses by differential scanning calorimeter, Phys. Chem. Glasses 20 (1979) 81–84.
[23] K. Matusita, S. Sakka, Kinetics study on crystallization of glass by differential thermal analysis-criterion on application of Kissinger plot, J. Non-Cryst. Solids 38-39 (1980) 741–746.
[24] N. Pallas, B. Pethica, Surface tension of water, Colloids Surfaces 6 (3) (1983) 221–227.
[25] P.W. Schindler, Surface Complexes at Oxide–Water Interface, Ann Arbor Science Publishers, Ann Arbor, MI, 1981.
[26] M.N. Rahaman, Ceramic Processing and Sintering, Marcel Dekker, Inc., New York, 1995.
[27] X.J. Luo, B.L. Zhang, W.L. Li, H.R. Zhuang, Preparation of aluminum nitride green sheet by aqueous tape casting, Ceram. Int. 30 (2004) 2099–2103.
[28] J.S. Reed, Principles of Ceramics Processing, John Wiley, New York, 1995.
[29] J.H. Feng, F. Dogan, Aqueous processing and mechanical properties of PLZT green tapes, Mater. Sci. Eng. A 283 (2000) 56–64.